

Mining for Candidates of Galactic Stellar-mass Black Hole Binaries with LAMOST

TUAN YI,¹ MOUYUAN SUN,¹ AND WEI-MIN GU¹

¹*Department of Astronomy, Xiamen University, Xiamen, Fujian 361005, P. R. China*

(Received; Revised; Accepted)

ABSTRACT

We study the prospects of searching for black hole (BH) binary systems with a stellar-mass BH and a non-compact visible companion, by utilizing the spectroscopic data of *Large Sky Area Multi-Object Fiber Spectroscopic Telescope* (LAMOST). We simulate the Galactic BH binary population and determine its optical visibility by considering the stellar synthetic population model and the distributions of binary orbital parameters. By convolving the visibility of BH binaries with the LAMOST detection sensitivity, we predict that $\gtrsim 400$ candidate BH binaries can be found by the low-resolution, non-time-domain survey, and ~ 50 -350 candidates by the LAMOST ongoing medium-resolution, time-domain spectroscopic survey. Most of the candidates are short-period (0.2-2 days) binaries with M-, K-, G-, or F-type companions, in which $\sim 47\%$ have a mass function (the lower limit of the BH mass) larger than $3 M_{\odot}$. By complementing the LAMOST spectroscopic data with other photometric/spectroscopic surveys or follow-up observations, these candidates could be confirmed. Therefore, by exploring the LAMOST data, we can enlarge the sample of dynamically confirmed BH binaries significantly, which can improve our understanding of the mass distribution of BHs and the stellar evolution model.

Keywords: binaries: general — stars: black holes — stars: kinematics and dynamics — radial velocities

1. INTRODUCTION

Stellar-mass black holes (BHs) are the ultimate fate of massive stars at the end of their life. According to stellar evolution model, there are around 10^8 - 10^9 stellar-mass BHs reside in the Galaxy (van den Heuvel 1992; Brown & Bethe 1994; Timmes et al. 1996; Agol et al. 2002). A significant amount of these dark objects are thought to exist in binary systems (i.e., a system with a BH and a non-compact companion star). So far, only about 60 of such systems were found (Corral-Santana et al. 2016). Most of the candidates are interacting X-ray binaries (McClintock, & Remillard 2006; Remillard & McClintock 2006), i.e., the BH can accrete gas from its closely orbiting donor companion.

If the BH and its non-compact companion are detached (Karpov, & Lipunov 2001; Yungelson et al. 2006), namely, they are still gravitationally bounded but the companion is not filling the Roche-lobe, no mass-transfer-induced X-ray emissions will arise. Examples of discovered isolated and detached BH binaries are rare (Casares et al. 2014; Minniti et al. 2015; Giesers et al. 2018), since these systems are hard to detect through the X-ray window. Recently, the potential of detecting BHs by the mission of *Gaia* was discussed intensively (Breivik et al. 2017; Mashian & Loeb 2017; Yalinewich et al. 2018; Yamaguchi et al. 2018). *Gaia* provides a dedicated way for hunting BHs by directly resolving the orbit astrometric signature (Gaia Collaboration et al. 2016). Mashian & Loeb (2017) estimated that 2×10^5 BHs could be hunted by *Gaia*, while Breivik et al. (2017) predicted a roughly consistent result of 3800-12000 BHs by synthetic stellar evolution simulation. Later, Yamaguchi et al. (2018) raised a key point that the effects of interstellar extinction ought to be considered, which leads to a more moderate estimation of discovering 200-1000 BHs. Another feasible way to identify short period candidates is looking for photometric data that present characteristics of microlensing and tidal

Table 1. The distributions adopted in this paper.

Quantity	Distribution	Reference
M_* (M_\odot)	Initial Mass Function (IMF, subscript 0 means ‘initial’): $\Psi_{M_0}(M_*) \propto \begin{cases} (M_*/0.5)^{-1.3} & 0.08 M_\odot \leq M_* < 0.5 M_\odot \\ (M_*/0.5)^{-2.3} & 0.5 M_\odot \leq M_* \leq 100 M_\odot \end{cases}$	Kroupa (2001)
M_{BH} (M_\odot)	BH mass distributions: fiducial model (a) $\Psi_{M_{\text{BH}}}(M_{\text{BH}}) = \left\{ A(M_{\text{BH}})^n + [B(M_{\text{BH}})^{-n} + C(M_{\text{BH}})^{-n}]^{-1} \right\}^{1/n}$ where: $n = -10.0$, $A(M_{\text{BH}}) = 4.367 - 1.7294M_{\text{BH}} + 0.1713M_{\text{BH}}^2$, $B(M_{\text{BH}}) = 14.24 \exp(-0.542M_{\text{BH}})$, $C(M_{\text{BH}}) = 3.322 \exp(-0.386M_{\text{BH}})$	Özel et al. (2010) Özel et al. (2012)
	BH mass distributions: alternative model (b) $\Psi_{M_{\text{BH}}}(M_{\text{BH}}) \propto \exp(-kM_{\text{BH}})$	Fryer & Kalogera (2001)
a (R_\odot)	Logarithmically-flat distributed separation: $\Psi_A(a) \propto 1/a, \quad 3 R_\odot \leq a \leq 10^4 R_\odot$	Abt (1983)
i	Randomly-distributed orbital orientation: $\Psi_I(i) = \text{Constant}, \quad 0 \leq i \leq \pi/2$	–
$n(r, \theta, \phi)$	Galactic stellar number density distribution: $n(r, \theta, \phi) = n_0 \left[\exp\left(-\frac{r \sin \phi + R_{\text{Sun}}}{2.6 \text{kpc}} - \frac{r \cos \phi + Z_{\text{Sun}}}{0.3 \text{kpc}}\right) + 0.04 \exp\left(-\frac{r \sin \phi + R_{\text{Sun}}}{3.6 \text{kpc}} - \frac{r \cos \phi + Z_{\text{Sun}}}{0.9 \text{kpc}}\right) \right]$ where: $n_0 \approx 3 \text{ pc}^{-3}$, $R_{\text{Sun}} = 8 \text{ kpc}$, $Z_{\text{Sun}} = 25 \text{ pc}$	Jurić et al. (2008) Mashian & Loeb (2017)

distortion effects (Wyrzykowski et al. 2016; Masuda & Hotokezaka 2018). From the spectroscopic perspective, the system of a BH plus a non-compact companion is a single-lined spectroscopic binary (SB1). The stellar spectra provide information of stellar parameters and radial velocities (V_R) for the visible companion. The mass function equation, derived from the radial velocity curve of the bright star, puts a robust lower limit to the mass of the unseen star (e.g. Casares & Jonker 2014). If the orbital inclination is obtained through fitting the photometric light curves by synthetic models (e.g. Orosz, & Hauschildt 2000; Beer, & Podsiadlowski 2002), and the binary mass ratio constrained through, for instance, resolving the rotational broadening of the photospheric lines from the visible companion (e.g. Marsh et al. 1994), the mass of the unseen object can be well determined.

The *Large Sky Area Multi-Object Fiber Spectroscopic Telescope* (LAMOST, Su & Cui 2004; Cui et al. 2012) is a unique astronomical instrument that has 4000 optical fibers assembled in the focal plane, allowing the spectrographs to take thousands of spectra simultaneously. The LAMOST Experiment for Galactic Understanding and Exploration (LEGUE; Deng et al. 2012) survey is mobilized with highly automated pipelines for sky subtraction (Bai et al. 2017b), cosmic ray removal (Bai et al. 2017a), data reduction and calibration (Song et al. 2012; Luo et al. 2014), and stellar parameters determination (Wu et al. 2011, 2014; Xiang et al. 2015). Since its first data release in 2013 (Luo et al. 2015), the LAMOST spectroscopic survey has provided more than 10 million stellar spectra to date, making it the largest stellar spectral database¹ ever. The ongoing LAMOST medium-resolution survey has released data of around 3,124,000 stellar spectra with $S/N_R > 10$ at its first and second observing campaign. The medium-resolution spectrographs have spectral resolution of $R \sim 7500$, and the precision of the radial velocity measurements can reach

¹ <http://dr7.lamost.org/>

1 km s⁻¹ for $S/N_R \sim 20$ (Liu et al. 2019). In the future, the ongoing LAMOST medium-resolution time-domain campaign will provide high-quality multi-epoch spectroscopic observations, i.e., each target will have more than 60 exposures. Thus the LAMOST spectroscopic database is an invaluable resource for mining BH binaries through the spectroscopic point of view, i.e., with radial velocity measurements that provide dynamical constraints for binary systems.

In this paper, we focus on the prospects of mining candidate BH binaries with LAMOST. This manuscript is organized as follows. In Section 2, we present our model. In Section 3, we show our results. Summary and discussions are made in Section 4.

2. THEORETICAL MODEL

In order to estimate the number of detectable BH candidates with LAMOST, we must solve the following three questions:

- (a) *Population*: how many BH binary systems with stellar companions reside in our Galaxy?
- (b) *Observability*: how many of these BH binaries are within the detection limits of LAMOST?
- (c) *Identifiability*: how many of these BH binaries have a signature of being identified as candidates?

The first question concerns the population and the evolution paths of the BH binaries. We start with some definitions that describe the orbital parameters of a binary system:

$M_{\min}=0.08 M_{\odot}$: minimum mass of a hydrogen burning star.

$M_{\max}=100 M_{\odot}$: maximal mass of a star that remains stable under the balance of stellar gravity and its radiation pressure.

$M_1 (M_{\odot})$: mass of the primary, the most massive component in the initially formed binary system.

$M_2 (M_{\odot})$: mass of the companion, the least massive component in the initially formed binary system ($M_{\min} \leq M_2 \leq M_1 \leq M_{\max}$ are satisfied).

$M_{\text{BH}} (M_{\odot})$: mass of the BH as the remnant of a progenitor that ends its life.

$q \equiv M_2/M_{\text{BH}}$: mass ratio of BH binary system.

$a (R_{\odot})$: orbital semi-major axis (binary separation).

P_{orb} (days): orbital period of the binary.

i : orbital inclination angle.

2.1. Population and Evolution Paths

To estimate the BH binary population, we develop a similar methodology to Mashian & Loeb (2017). It is widely believed that more than $\sim 50\%$ of stars reside in binary systems (Duchêne, & Kraus 2013; Yuan et al. 2015). For massive early-type stars, the binary fraction even reaches $\sim 70\%$ in the open clusters (Sana et al. 2012). BHs with stellar companions can be formed by different stellar evolution channels (Belczynski et al. 2002; Heger et al. 2003). Typically, a massive progenitor with mass $\gtrsim 20M_{\odot}$ at its final evolution stage will explode as a supernova (SN) and give birth to a remnant BH by fallback accretion onto the collapsing core. SN could lead to the destruction of the binary by the natal kick that unbinds the remnant compact object and its companion (Fryer et al. 2012). According to a recent study (Kochanek et al. 2019) on surviving star plus remnant binaries in a sample of 49 SN remnants, $\lesssim 0.1$ SN remnants contain a binary, while the binary population synthesis models (Belczynski et al. 2008) predict that only $\sim 5\%$ of the star plus remnant binaries eventually survive the SN. More massive progenitor with mass $\gtrsim 40M_{\odot}$ may directly collapse into a BH without experiencing an SN explosion. If we consider a Kroupa (2001) initial mass function (IMF, Table 1, first row), the fraction of binaries that end up as a BH and a visible stellar companion is:

$$f_{\text{BHB}} = 0.5 \times (f_{\text{s}} \int_{20M_{\odot}}^{40M_{\odot}} \Psi_{M_0}(M_*)dM_* + \int_{40M_{\odot}}^{100M_{\odot}} \Psi_{M_0}(M_*)dM_*), \quad (1)$$

where the factor 0.5 is assumed as the fraction of the binaries in the Galaxy, namely, there are 50 binaries and 50 single stars in 150 stars. f_{s} is the fraction of binaries that survived the SN explosion, and $\Psi_{M_0}(M_*)$ is the IMF with M_* denoting the stellar mass. We assume $f_{\text{s}} = 0.05$. The integration yields $f_{\text{BHB}} \approx 0.0003$, i.e., roughly three BH binaries exist in every ten thousand stars.

In order to detect the BH binaries via LAMOST, the non-compact companion should be still shining. Following Mashian & Loeb (2017), we calculate the fraction of stars that are still shining as follows,

$$f_{\text{shinning}} = 1 - \frac{\rho_*(z(t_{\text{LB}} = t_{\text{age}}(M_*)))}{\rho_*(0)}, \quad (2)$$

where M_* , $\rho_*(z)$, t_{LB} and $t_{\text{age}}(M_*)$ are the stellar mass, the comoving mass density², the look-back time³, and the age of the star, respectively. Following Mashian & Loeb (2017), we also integrate the star formation history (Madau, & Dickinson 2014; Madau, & Fragos 2017) of the Universe to obtain $\rho_*(z)$; the age of the star is estimated by using the analytical formula (Equation (4)) in Hurley et al. (2000). Hence the stellar mass distribution (SMF) $\Psi_{M_2}(M_*)$ of the visible companion at present ($z=0$) is:

$$\Psi_{M_2}(M_*) \propto f_{\text{shinning}}(M_*) \Psi_{M_0}(M_*). \quad (3)$$

Shown in the left panel of Figure 1 are the IMF (dashed line) and the SMF (solid line).

The observability is also affected by the spatial distribution of BH binaries. For simplicity, we assume that the spatial distribution of the binaries traces the distribution of the stars in the Milky Way, which can be modeled as a double exponential thick and thin disk model (Gilmore, & Reid 1983; Jurić et al. 2008). The adopted normalized number density profile is shown in Table 1 (last row; Mashian & Loeb 2017).

It should be noted that during the evolution, binary interactions (e.g. Hurley et al. 2002) can change the component masses and the orbital separation. Processes such as mass loss by the stellar wind, mass transfer, mass accretion, and common envelope (CE) evolution (e.g. Paczynski 1976; Iben, & Livio 1993; Ivanova et al. 2013) are not included in the current work for simplicity. Binaries that have evolved through the CE phase may have an orbital period (separation) orders of magnitude smaller than the initial period (separation), since most of the angular momentum is taken away by the envelope (Paczynski 1976). We take a detour by adopting a logarithmically flat distribution for the orbital separation (Table 1, row 3; Abt 1983). The distribution can approximate the real cases, as it is a statistically summarized result from observations.

2.2. Mass Distributions of BHs

As for the mass distribution of BHs, we adopt the distribution of Özel et al. (2010, 2012) as a fiducial one (hereafter referred to *Fiducial* model). Özel et al. (2010) derived a BH mass distribution from dynamical mass measurements of 16 BHs in transient low-mass X-ray binaries. The distribution peaks at around $7 M_{\odot}$, and presents a mass gap ($2\text{-}5 M_{\odot}$; see also Bailyn et al. 1998; Farr et al. 2011; Belczynski et al. 2012) between the population of BH and the most massive neutron star. We also propose an alternative distribution for the purpose of comparison. Our distribution is motivated by Fryer & Kalogera (2001), who studied the compact remnants masses by analyzing the balance between the stellar bounding energy and supernova explosion energy. Fryer & Kalogera (2001) found that the BH mass distribution falls off exponentially. Thus, we assume the BH mass distribution takes the form:

$$\Psi_{M_{\text{BH}}}(M_{\text{BH}}) \propto \exp(-kM_{\text{BH}}) \quad (4)$$

where the exponential factor k is taken to be 0.1, 0.2, 0.3 in the calculation. Both distributions are shown in Table 1 (second row) and plotted in the right panel of Figure 1.

2.3. Observational Cuts

The low-resolution spectrographs of LAMOST are capable of observing stars with an average limiting magnitude $m_V^L \sim 18$ mag in V -band and a precision $V_R^{\text{pre}} = 5$ km s⁻¹ for radial velocity (V_R) measurements (Deng et al. 2012). The detection limits for medium-resolution spectrographs are: $m_V^L \sim 15$ mag and $V_R^{\text{pre}} = 1$ km s⁻¹ (Liu et al. 2019). The sky footprint of LAMOST is $-\pi/18 < \delta < \pi/3$ (δ : the declination) in the equatorial coordinate (Zhao et al. 2012).

To estimate the apparent brightness of binaries, we assume the mass-luminosity relation $L = M_{\text{ZAMS}}^{3.5}$ for zero-age main sequence (ZAMS) star. Therefore, for a fixed distance d (in units of pc), there is a lower limit of the mass of the stars that are bright enough to be captured by LAMOST, i.e., this lower mass limit is:

$$M_{\text{min}}^d = \left(\left(\frac{d}{10 \text{ pc}} \right)^2 10^{\frac{M_V^{\text{Sun}} - m_V^L + A_V(d)}{2.5}} \right)^{\frac{1}{3.5}}, \quad (5)$$

² comoving mass density: the stellar mass density at redshift z .

³ look-back time: the cosmological time at redshift z .

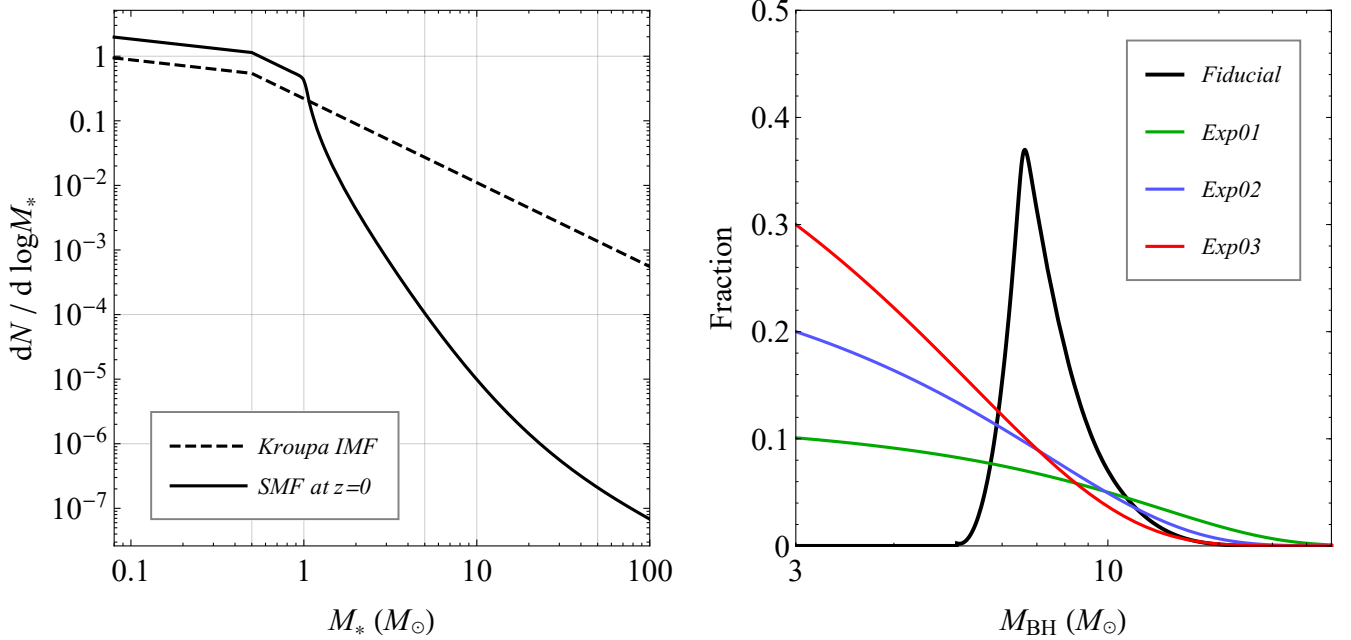


Figure 1. Left panel: the IMF (dashed line) and the SMF (solid line). Right panel: The fiducial BH mass distribution adopted from Özel et al. (2010, black), and the alternative exponential distributions motivated by Fryer & Kalogera (2001): *Exp01* (green), *Exp02* (blue), and *Exp03* (red) correspond to the exponential factor $k=0.1, 0.2,$ and $0.3,$ respectively. All distributions are normalized to make sure the integration over the mass range equals unity.

where $M_V^{\text{Sun}} = 4.83$ is the absolute magnitude of the Sun, and $A_V(d)$ is the interstellar extinction. Following Yamaguchi et al. (2018), we adopt the average extinction of the Galactic disk: $A_V(d) = d/(1 \text{ kpc})$ (Spitzer 1978).

There is also an accessible range of the radial velocity curve semi-amplitude K_2 , given the precision of V_R measurements. From Kepler’s third law, the semi-amplitude K_2 is:

$$K_2 = \left(\frac{GM_{\text{BH}}}{a(1+q)} \right)^{\frac{1}{2}} \sin i . \quad (6)$$

For the orbital inclination i , we assume that the binary orbits are randomly distributed (Table 1, row 4). The circular orbit assumption (zero eccentricity) is also assumed.

Let us define $\Psi_{K_2}(k)$ as the probability distribution function (PDF) and $\Phi_{K_2}(k)$ as the cumulative distribution function (CDF) of K_2 . By definition,

$$\begin{aligned} \Phi_{K_2}(k) = \text{Prob}(K_2 \leq k) &= \int_{K_2 \leq k} \Psi_A(a) \Psi_{M_{\text{BH}}}(m) \Psi_Q(q) \Psi_I(i) da dm dq di , \\ \Psi_{K_2}(k) &= \frac{d}{dk} \Phi_{K_2}(k) \end{aligned} \quad (7)$$

where $\text{Prob}(K_2 \leq k)$ is the probability of a specific binary system whose amplitude K_2 is less than or equal to a measured value k .

We assure the reliability of K_2 measurements by putting a lower cut K_2^{min} of 10 times V_R^{pre} . In other words, the reliable measured K_2 should be $> 50 \text{ km s}^{-1}$ for low-resolution spectrograph, and $> 10 \text{ km s}^{-1}$ for medium-resolution spectrograph. So to acquire a proper error estimation of the amplitude K_2 , i.e., for a radial velocity curve with semi-amplitude $K_2 > K_2^{\text{min}} = 50 \text{ km s}^{-1}$ taken by the low-resolution spectrograph, the uncertainty of K_2 is $< 5 \text{ km s}^{-1}$ provided that the average V_R uncertainty = 5 km s^{-1} .

Table 2 summarizes the observational cuts for the LAMOST surveys.

Table 2. Observational cuts

survey	R	m_V^L (*)	K_2^{\min}	δ
		(mag)	(km s ⁻¹)	(radians)
(1)	(2)	(3)	(4)	(5)
low-resolution	~ 1800	18	50	$-\frac{\pi}{18} \sim \frac{\pi}{3}$
medium-resolution	~ 7500	15	10	$-\frac{\pi}{18} \sim \frac{\pi}{3}$

NOTE—Column (1): the LAMOST surveys. Column (2): the resolution of the spectrographs. Column (3): the detection limit. Column (4): the detection limit of the V_R semi-amplitude. Column (5): the equatorial latitude. (*): The LAMOST low resolution survey can capture spectra for stars brighter than $r \lesssim 19$ (r -band) during dark/grey time, and $r \lesssim 17$ or $J \lesssim 16$ on nights that are moonlit or have low transparency (Deng et al. 2012).

2.4. The Total Number of Candidates

Based on the knowledge discussed above, the number of detectable BH binary candidates can be estimated by a multi-dimensional integral:

$$N = f_{\text{BHB}} \times \int_{\text{Min}[100, M_{\min}^d]}^{100M_{\odot}} f_{\text{shinning}}(M_*) \Psi_{M_0}(M_*) dM_* \times \int_{-\pi/18 < \delta < \pi/3} \int \int \sin \phi d\phi d\theta \int_0^d r^2 dr n(r, \theta, \phi) \times \int_{10V_R^{\text{pre}}}^{\infty} \Psi_{K_2}(k) dk \times f_{\text{cad}}, \quad (8)$$

where the coefficient f_{BHB} is introduced in Equation (1). The first integral constrains the fraction of visible stars that do not exceed LAMOST’s detection threshold, the integrand is introduced at Equation (3), which calculates the fraction of stars that are still shining today by evolving the stellar population. The lower limit of the first integral is calculated by using Equation (5). The second, third, and fourth integrals sum up the stellar number density in the Galactic coordinate system, with the constraint of the equatorial declination: $-\pi/18 < \delta < \pi/3$. The transformation of this LAMOST visible sky region from equatorial to Galactic coordinate system is calculated by using Equations (1)-(4) in Poleski (2013). The fifth integral is the fraction of the accessible range of K_2 . The last term f_{cad} in the equation is defined as the fraction of sources with no less than three observations (spectra). In our opinion, three observations is a necessary condition to set constraints on K_2 .

2.5. Discovering and Confirming a BH

So far we have covered the first (population) and the second (observability) motivating questions given at the beginning of Section 2. Now, discovering a potential candidate BH is one thing, confirming (identifying) is another. Strategies are required to search for candidate BHs from large spectroscopic surveys. Notably, Gu et al. (2019) adopted the relation of the stellar radius and the Roche-lobe radius to constrain the binary separations, and used a few (≥ 3) V_R measurements to constrain the lower limit of V_R excursions. Their method was applied to search for BH candidates with LAMOST DR6. Thompson et al. (2018) developed a strategy based on the maximum acceleration of the system, to select potential candidates in SDSS APOGEE survey which has in average 2-4 measurements per system. If one has sufficient V_R measurements, the radial velocity curve and hence the mass function can be obtained. However, only a fraction of sources have intense observations in the LAMOST low-resolution survey. For example, $\sim 6\%$ of targets have three or more low-resolution visits in the LAMOST *Kepler* field (spanning five years from 2012 to 2017; Zong et al. 2018, Table1). In this case, complementary follow-up spectroscopic and photometric observations are required to measure the orbital periods. For instance, Zheng et al. (2019) searched for BH candidates with orbital periods revealed by the ASAS-SN photometry.

3. RESULTS AND ANALYSES

Figure 2 shows the distribution (PDF) and cumulative distribution (CDF) of visible companion’s mass and mass function for the detectable BH binaries by LAMOST. The left panel is the PDF and CDF of the mass of detectable

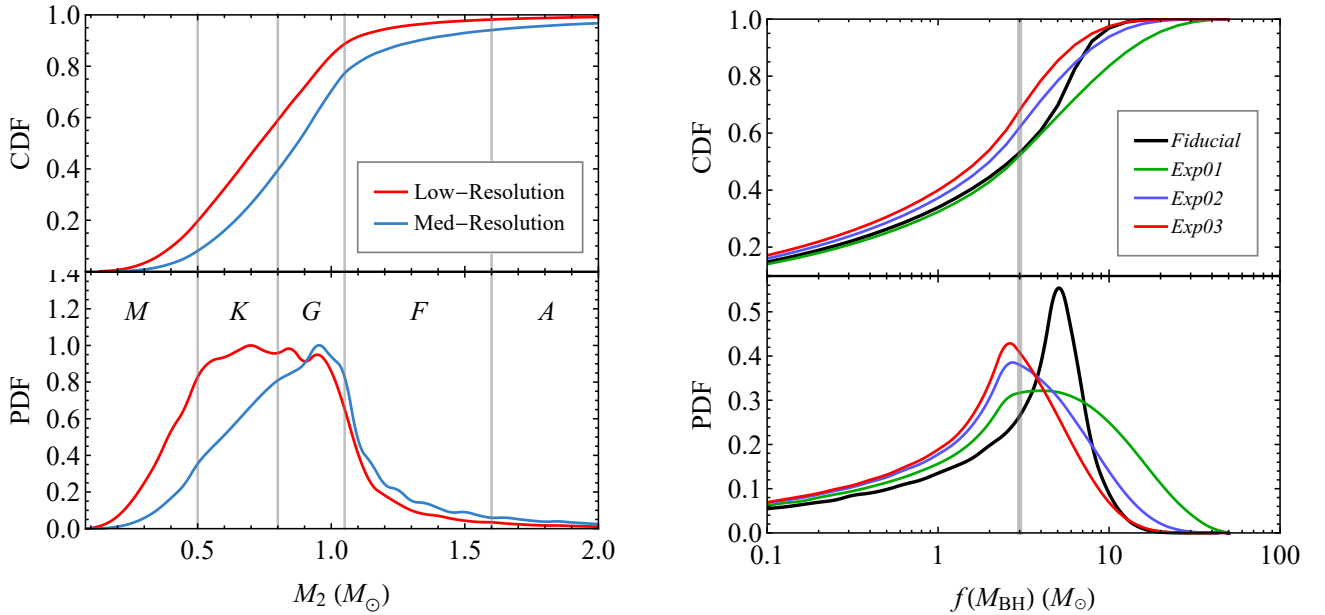


Figure 2. The distribution (PDF) and cumulative distribution (CDF) of the visible companion’s mass and mass function for the detectable BH binaries by LAMOST. Left panel: The PDF and CDF of the visible companion’s mass, for low- and medium-resolution spectrographs, respectively. Most of the expected candidates have a visible companion of M-, K-, G-, or F-type star. Right panel: The PDF and CDF of the BH binary mass function. Around 47% of the BH binaries have a mass function larger than $3 M_{\odot}$ (gray shallow line) for *Fiducial* model.

visible companions. The distributions are calculated with equally spaced sampling points in the linear space of M_2 , with a bin size of $0.05 M_{\odot}$. By using Equation (8), we first calculate the number of BH binaries and the fraction of the observable companions per mass bin at different distances, ranging from 20 pc to 5 kpc, then we sum up the number of each mass bin at all distances to find the fractions. The red and blue lines represent the low- and medium-resolution spectrographs, respectively. As suggested in the CDF, most of the detectable candidates are low-mass BH binaries with M-, K-, G- or F-type stars (MK system; Morgan, & Keenan 1973), i.e., for low-resolution spectrographs, the fractions for M-, K-, G- and F-type stars are $\sim 19.7\%$, $\sim 39.3\%$, $\sim 29.7\%$, and $\sim 9.5\%$, respectively. The resulting fractions are a natural consequence of the relative number of stars with a given spectral type (Chabrier 2003), plus the modification by the detection limits of LAMOST, i.e., fainter M-type stars are harder to be detected, hence the fraction is quenched. As for massive early-type (O, B) stars, the fraction of shining ones is tiny because of the short life time scale of these populations. As mentioned in Section 2, however, binary fractions may be higher ($\sim 70\%$) for early-type stars. Consequently, f_{BHB} is evaluated to be ~ 0.0004 in Equation (1), suggesting that the population of BH plus early-type young star binaries may be underestimated.

As discussed in Section 1, the binary mass function⁴ is useful to constrain a lower mass limit of the unseen object in the SB1 system (Casares & Jonker 2014). The binary mass function for a BH system is given by:

$$f(M_{\text{BH}}) = \frac{M_{\text{BH}} \sin^3 i}{(1+q)^2} = \frac{K_2^3 P_{\text{orb}}}{2\pi G}. \quad (9)$$

The right-hand side of the equation hints that $f(M_{\text{BH}})$ can be calculated by K_2 and P_{orb} , which are measurable quantities from the radial velocity curve.

⁴ Note the difference between the initial mass function (IMF) and the binary mass function: the IMF describes the mass distribution of the Galactic stellar population, while the binary mass function is a measurable quantity for a specific SB1 system, the lower mass limit of the unseen companion.

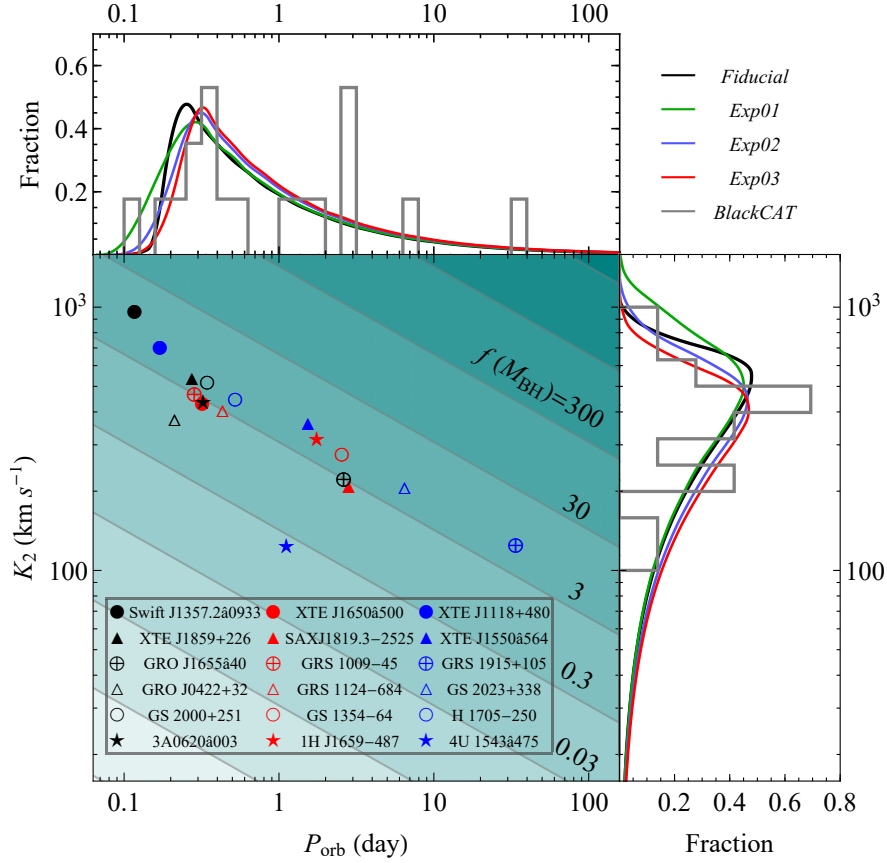


Figure 3. The distributions of orbital period P_{orb} and radial velocity amplitude K_2 for visible companion. Gray histograms denote the distributions of 18 dynamically confirmed BHs. Data of K_2 and P_{orb} are adapted from BlackCAT (Corral-Santana et al. 2016, Table A.4., columns 3 and 4). The contours corresponding to $f(M_{\text{BH}}) = 0.03, 0.3, 3, 30,$ and 300 are also draw in the figure.

The right panel of Figure 2 shows the PDF and CDF of the mass function. The distributions are calculated with equally spaced sampling points in the logarithmic space of $f(M_{\text{BH}})$, with a step size of $0.1 M_{\odot}$. Comparing to the results derived from *Exp* model, the one from *Fiducial* model rises more rapidly when passing $3 M_{\odot}$, peaks at around $5 M_{\odot}$, and falls off more rapidly with increasing mass. The vertical shallow gray line shows the BH binary system with $f(M_{\text{BH}}) = 3 M_{\odot}$. Note that BH binaries may have a $f(M_{\text{BH}}) < 3 M_{\odot}$. For instance, the mass function $f(M_{\text{BH}})$ of SAXJ1819.3-2525 is $2.7 \pm 0.1 M_{\odot}$ (V4641 Sgr, Orosz et al. 2001; MacDonald et al. 2014). In a practical perspective, if a SB1 system has mass function significantly larger than the mass of the visible star, the unseen star must be a compact object. In the calculation, we find that $\sim 47\%$, $\sim 48\%$, $\sim 38\%$, and $\sim 32\%$ of the BH binaries have mass functions larger than $3 M_{\odot}$, for the *Fiducial*, *Exp01*, *Exp02*, and *Exp03* models, respectively.

The distributions of the spectroscopic observables P_{orb} and K_2 are predicted and compared to 18 dynamically confirmed BHs (Corral-Santana et al. 2016). The distributions of the K_2 values are calculated by Equation (7). By implementing Kepler’s third law, the distribution of P_{orb} values, for the fiducial and exponential M_{BH} models, is derived from the distribution of orbital separations a (Table 1, row 3). Figure 3 shows the smoothed PDFs of P_{orb} and K_2 . Gray histogram denotes the corresponding distribution (fractional counts in the logarithmic space with a uniform step size = 0.1) of the 18 dynamically confirmed BHs. Data of K_2 and P_{orb} are adapted from BlackCAT (Corral-Santana et al. 2016, Table A.4., columns 3 and 4). The contours corresponding to $f(M_{\text{BH}}) = 0.03, 0.3, 3, 30,$ and 300 are also draw in the figure.

The orbital period distributions peak at around 0.23 (*Fiducial*)-0.3 (*Exp01*) days, with $\sim 76\%$ (*Exp01*)- 78% (*Fiducial*) binaries in the range 0.2-2 days, indicating that short period BH candidates are quite common in the observational

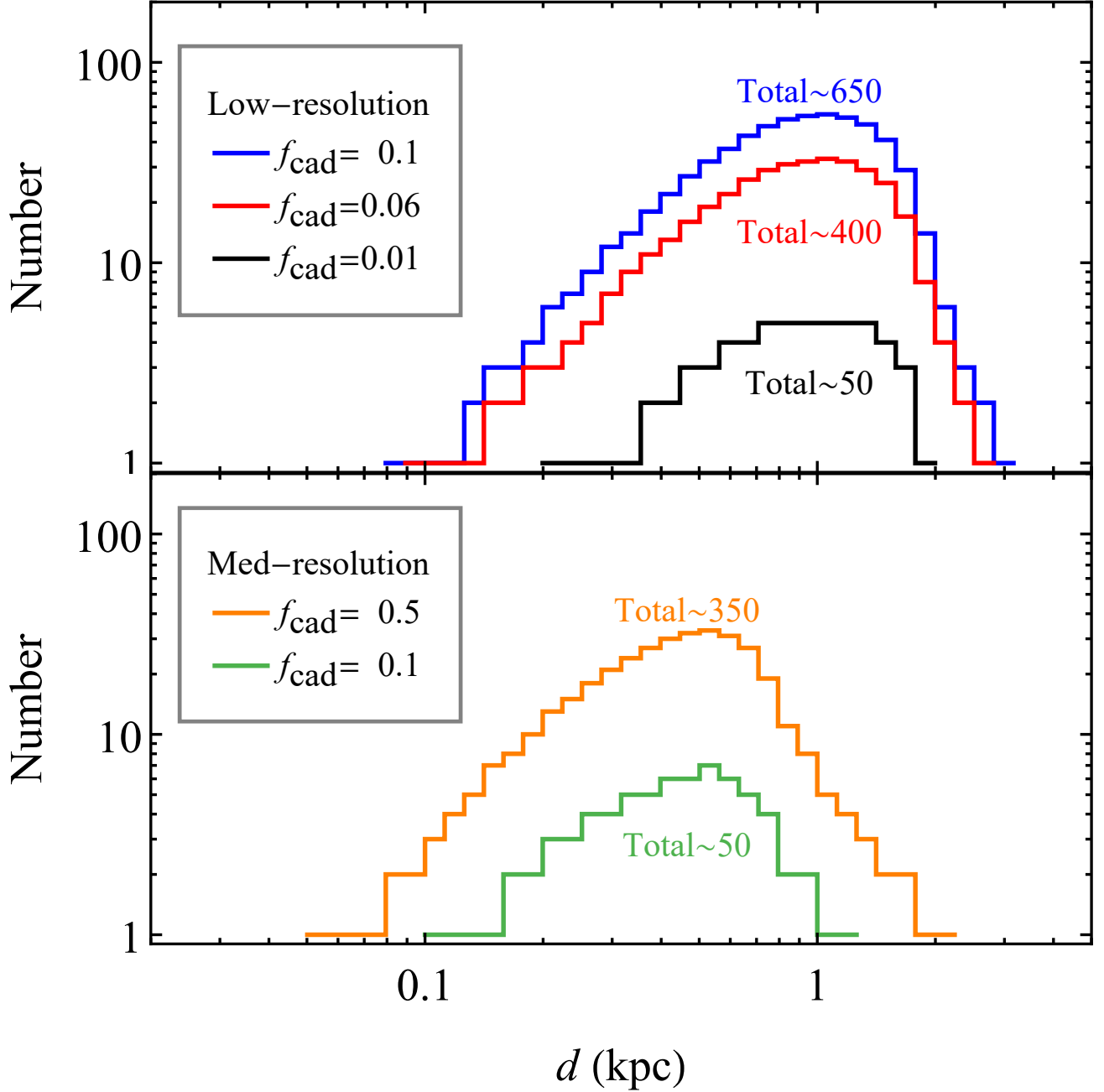


Figure 4. The number of detectable candidates as a function of distance. The blue, red and black lines represent the expected results by LAMOST low-resolution, non-time-domain survey, with $f_{\text{cad}} = 0.1, 0.06$, and 0.01 , respectively. The orange and green lines represent the expected results by medium-resolution, time-domain survey, with $f_{\text{cad}} = 0.5$, and 0.1 , respectively. The total predicted numbers of each case are rounded to the nearest 50s.

space of parameters. This implies that a large fraction will be quiescent BH transients, i.e., interacting binaries with accretion disks. Quiescent BH transients can be easily identified from the presence of broad emission lines, chiefly H_{α} . In some cases, such as Swift J1357-0922 (Mata Sánchez et al. 2015), the companion star is overwhelmed by the accretion disk light and, consequently, no radial velocity information can be obtained. In these cases, surveys exploiting the detection and properties of the H_{α} line (Casares 2015, 2018) can be very useful.

Table 3. The distributions of K_2 in linear space.

Model	Fractions of K_2 at different range (km s ⁻¹)					
	< 200	200-400	400-600	600-800	800-1000	>1000
<i>Fiducial</i>	0.355	0.328	0.245	0.068	0.003	0
<i>Exp01</i>	0.327	0.302	0.218	0.102	0.040	0.011
<i>Exp02</i>	0.392	0.346	0.200	0.052	0.009	0.001
<i>Exp03</i>	0.428	0.368	0.175	0.027	0.002	0

Regarding the radial velocity semi-amplitude K_2 distribution, the results show a peak at around 500 - 600 km s⁻¹. We also present the calculated fractions in linear space, as presented in Table 3. It shows that the fraction of K_2 values under 400 km s⁻¹ is larger than the fraction above, indicating that there is a good chance of detecting BH binaries with $K_2 < 400$ km s⁻¹ (even for $K_2 < 200$ km s⁻¹, the odds are still good). Note that extremely large $K_2 \sim 1000$ km s⁻¹ might be possible. These are close pairs that contain a low-mass dwarf (M dwarf) star and a BH with $M_{\text{BH}} \gtrsim 30 M_{\odot}$. The BHs could form through the direct collapse of massive O stars or Wolf-Rayet Stars, without experiencing a supernova explosion and thus barely losing any mass.

We calculate Equation (8) by setting $f_{\text{cad}}=0.06$ (see Section 2) for the low-resolution survey; $f_{\text{cad}}=0.1$ is also considered, since as the survey lasts, more spectra will be accumulated for most of the sources; and $f_{\text{cad}}=0.01$, to including less optimistic estimation. As for the medium-resolution time-domain survey, sufficient observational epochs are guaranteed (~ 60 visits for every single target), leading to a tentative value of $f_{\text{cad}}=1$. However, the value of f_{cad} is unknown, so we take $f_{\text{cad}} = 0.5$ and 0.1 for illustrative purposes. Shown in the Figure 4 is the expected number of detectable candidates as a function of distance. The calculation step size is 0.05 in logarithmic space of distance d . We present only the results derived from *Fiducial* distribution as *Exp* one gives same results. The blue, red, and black lines represent the results by LAMOST low-resolution, non-time-domain survey, for $f_{\text{cad}} = 0.1, 0.06,$ and 0.01 , respectively. The total number of each case are rounded to the nearest 50 s, shown on top / below the lines (with the same color to the lines). The number rises with increasing distance in the first place, as the number of stars increases with the increasing volume. The maximum number of the expected candidates is located near 1 kpc. At larger distances, the telescope gradually loses faint stars because of the detection limit plus the effect of the Galactic extinction. The number falls off beyond 1 kpc, with the farthest candidates located at ~ 3 kpc. We expect ~ 400 candidates to be found by the low-resolution survey, depending on the actual value of f_{cad} . The orange and green lines represent the expected results by the medium-resolution, time-domain survey, for $f_{\text{cad}} = 0.5,$ and $0.1,$ respectively. Compared to the low-resolution survey that can go deeper, the medium-resolution survey can only catch stars that are brighter than 15 mag in the V-band, hence most of the candidates are expected to be located within 2 kpc. We expect ~ 50 -350 candidates to be found as the medium-resolution time-domain survey lasts. The results show that both the low-resolution and medium-resolution surveys will enlarge the size of current dynamically confirmed catalog by an order of magnitude.

4. CONCLUSIONS AND DISCUSSION

In this paper, we study the prospects of searching for binary systems with a stellar-mass BH and a non-compact visible companion, by utilizing the spectroscopic data of LAMOST. Our results can be summarized as follows.

- Most of the expected candidates have a visible companion of M-, K-, G-, or F-type star.
- About 47 % of these BH binaries have a mass function larger than $3 M_{\odot}$.
- A majority of candidates have an orbital period in between 0.2-2 days, suggesting that the discovery of short period BH binaries is favored.
- Most of the detectable BH candidates are located within 2 kpc of the solar neighborhood.
- We predict that $\gtrsim 400$ candidate BH binaries can be found by the low-resolution, non-time-domain survey, and \sim

50-350 candidates by the LAMOST ongoing medium-resolution, time-domain spectroscopic survey. The results show that both low- and medium-resolution surveys are promising to enlarge the size of current dynamically confirmed catalog by an order of magnitude.

We would like to address a caveat for the theoretical analyses in this work. As mentioned in Section 2.1, binary interactions such as CE evolution are neglected for simplicity. However, the impact on results remains uncertain. For example, the CE phase can cause uncertainty on the second term in the right-hand side of Equation (1). More specifically, in systems with large mass ratios, binaries with a massive progenitor and a low-mass late-type companion may eventually merge, since the low-mass companion cannot take the burden of the CE mass ejection. These systems thus have no contribution to the population of interest. Hence the CE phase can reduce the population of BH binaries and hence decrease the discovery rates. Binary population synthesis is needed for obtaining more precise results.

Recently, several works (Breivik et al. 2017; Mashian & Loeb 2017; Yalınewich et al. 2018; Yamaguchi et al. 2018) have investigated the ability to dynamically detect BH binaries by *Gaia* satellite. The *Gaia* astrometric measurements resolve the orbital motion of the visible star, such robust observations allow one to solve the mass of unseen object simply by Kepler’s third law. Since *Gaia* has a unique strategy of sky-scanning that is designed for optimizing the astrometric accuracy, it is better at detecting long period binaries ($\gtrsim 30$ days) over short period ones. At this point, LAMOST has the advantage of observing binary systems with a wider range of orbital periods. For each target, LAMOST takes three (or more) exposures in a single observation, and each exposure takes 10-30 minutes. Each target will be covered ~ 60 times during the course of the entire time-domain survey. Hence LAMOST is capable of tracking short period binaries down to a few hours, or hunting long period binaries up to years.

As mentioned in Section 2, the potential of mining BH binaries from spectroscopic observations can be reinforced with follow-up spectroscopic and photometric observations. In fact, dynamically confirmed BHs are studied through both their spectroscopy and photometry (e.g. Orosz, & Bailyn 1997; McClintock et al. 2001; Wu et al. 2016). On one hand, spectra provide information for the visible star’s radial velocities, spectral types, and possible signature from an accretion disk (broad H_α emission line); on the other hand, light curves from photometric measurements provide valuable information for the orbital period, orbital inclination, and the mass ratio of the binary (in the case of extreme mass ratio, q can be best obtained from resolving the rotational broadening ($V \sin i$) of the donor star (e.g. Marsh et al. 1994)). It implies a novel approach for hunting a BH via the optical point of view: (a) Start from picking out SB1 sources with large radial velocity excursions, inspect whether broad emission lines are present. (b) Cross-match suspected sources with other spectroscopic and photometric surveys, set constraints upon the orbital period or the binary separation. (c) Calculate the mass function of the unseen companion and select candidates that have a mass function $f(M_{\text{BH}}) > 3 M_\odot$. (d) Collect data from follow-up observations and measure the full set of orbital parameters that shall confirm candidates and put final constraints on the BH masses.

We thank Hao-Tong Zhang, Zhong-Rui Bai, Wei-Kai Zong, Xuefei Chen, and Hailiang Chen for beneficial discussion, and thank the anonymous referee for giving numerous detailed, helpful suggestions that improved the manuscript. This work was supported by the National Natural Science Foundation of China under grants 11573023, 11603022 and 11973002, and the Fundamental Research Funds for Xiamen University under grants 20720190122 and 20720190115. Guoshoujing Telescope (the Large Sky Area Multi-Object Fiber Spectroscopic Telescope, LAMOST) is a National Major Scientific Project built by the Chinese Academy of Sciences. Funding for the project has been provided by the National Development and Reform Commission. LAMOST is operated and managed by the National Astronomical Observatories, Chinese Academy of Sciences.

REFERENCES

- Abt, H. A. 1983, ARA&A, 21, 343
- Agol, E., Kamionkowski, M., Koopmans, L. V. E., & Blandford, R. D. 2002, ApJL, 576, L131
- Bai, Z., Zhang, H., Yuan, H., et al. 2017, PASP, 129, 024004
- Bai, Z.-R., Zhang, H.-T., Yuan, H.-L., et al. 2017, Research in Astronomy and Astrophysics, 17, 091
- Bailyn, C. D., Jain, R. K., Coppi, P., et al. 1998, ApJ, 499, 367.
- Beer, M. E., & Podsiadlowski, P. 2002, MNRAS, 331, 351.
- Belczynski, K., Kalogera, V., & Bulik, T. 2002, ApJ, 572, 407.
- Belczynski, K., Kalogera, V., Rasio, F. A., et al. 2008, ApJS, 174, 223.

- Belczynski, K., Wiktorowicz, G., Fryer, C. L., et al. 2012, *ApJ*, 757, 91.
- Breivik, K., Chatterjee, S., & Larson, S. L. 2017, *ApJL*, 850, L13
- Brown, G. E., & Bethe, H. A. 1994, *ApJ*, 423, 659
- Casares, J., & Jonker, P. G. 2014, *SSRv*, 183, 223
- Casares, J., Negueruela, I., Ribó, M., et al. 2014, *Nature*, 505, 378
- Casares, J. 2015, *ApJ*, 808, 80
- Casares, J. 2018, *MNRAS*, 473, 5195
- Casares, J., & Torres, M. A. P. 2018, *MNRAS*, 481, 4372
- Chabrier, G. 2003, *PASP*, 115, 763.
- Corral-Santana, J. M., Casares, J., Muñoz-Darias, T., et al. 2016, *A&A*, 587, A61
- Cui, X.-Q., Zhao, Y.-H., Chu, Y.-Q., et al. 2012, *Research in Astronomy and Astrophysics*, 12, 1197
- Deng, L.-C., Newberg, H. J., Liu, C., et al. 2012, *Research in Astronomy and Astrophysics*, 12, 735.
- Duchêne, G., & Kraus, A. 2013, *ARA&A*, 51, 269.
- Farr, W. M., Sravan, N., Cantrell, A., et al. 2011, *ApJ*, 741, 103.
- Fryer, C. L., & Kalogera, V. 2001, *ApJ*, 554, 548
- Fryer, C. L., Belczynski, K., Wiktorowicz, G., et al. 2012, *ApJ*, 749, 91.
- Gaia Collaboration, Prusti, T., de Bruijne, J. H. J., et al. 2016, *A&A*, 595, A1.
- Giesers, B., Dreizler, S., Husser, T.-O., et al. 2018, *MNRAS*, 475, L15
- Gilmore, G., & Reid, N. 1983, *MNRAS*, 202, 1025
- Gu, W.-M., Mu, H.-J., Fu, J.-B., et al. 2019, *ApJ*, 872, L20.
- He, B., Fan, D., Cui, C., et al. 2016, arXiv:1601.02334
- Heger, A., Fryer, C. L., Woosley, S. E., et al. 2003, *ApJ*, 591, 288.
- Hogeveen, S. J. 1992, *Ap&SS*, 196, 299
- Hurley, J. R., Pols, O. R., & Tout, C. A. 2000, *MNRAS*, 315, 543
- Hurley, J. R., Tout, C. A., & Pols, O. R. 2002, *MNRAS*, 329, 897.
- Iben, I., & Livio, M. 1993, *PASP*, 105, 1373.
- Ivanova, N., Justham, S., Chen, X., et al. 2013, *A&A Rv*, 21, 59.
- Jiang, Z., Wang, J., Gao, L., et al. 2019, arXiv e-prints , arXiv:1904.11224.
- Jurić, M., Ivezić, Ž., Brooks, A., et al. 2008, *ApJ*, 673, 864.
- Karpov, S. V., & Lipunov, V. M. 2001, *Astronomy Letters*, 27, 645.
- Kinugawa, T., & Yamaguchi, M. S. 2018, arXiv:1810.09721
- Kochanek, C. S., Auhettl, K., & Belczynski, K. 2019, *MNRAS*, 485, 5394.
- Kroupa, P. 2001, *MNRAS*, 322, 231
- Liu, N., Fu, J.-N., Zong, W., et al. 2019, arXiv:1901.00619
- Luo, A., Zhang, J., Chen, J., et al. 2014, *Setting the Scene for Gaia and LAMOST*, 428
- Luo, A.-L., Zhao, Y.-H., Zhao, G., et al. 2015, *Research in Astronomy and Astrophysics*, 15, 1095
- MacDonald, R. K. D., Baily, C. D., Buxton, M., et al. 2014, *ApJ*, 784, 2.
- Madau, P., & Dickinson, M. 2014, *ARA&A*, 52, 415.
- Madau, P., & Fragos, T. 2017, *ApJ*, 840, 39.
- Marsh, T. R., Robinson, E. L., & Wood, J. H. 1994, *MNRAS*, 266, 137
- Mashian, N., & Loeb, A. 2017, *MNRAS*, 470, 2611
- Masuda, K., & Hotokezaka, K. 2018, arXiv:1808.10856
- Mata Sánchez, D., Muñoz-Darias, T., Casares, J., et al. 2015, *MNRAS*, 454, 2199
- McClintock, J. E., Garcia, M. R., Caldwell, N., et al. 2001, *ApJ*, 551, L147.
- McClintock, J. E., & Remillard, R. A. 2006, *Compact Stellar X-ray Sources*, 157.
- Minniti, D., Contreras Ramos, R., Alonso-García, J., et al. 2015, *ApJL*, 810, L20
- Morgan, W. W., & Keenan, P. C. 1973, *ARA&A*, 11, 29.
- Orosz, J. A., & Bailyn, C. D. 1997, *ApJ*, 477, 876.
- Orosz, J. A., & Hauschildt, P. H. 2000, *A&A*, 364, 265.
- Orosz, J. A., Kuulkers, E., van der Klis, M., et al. 2001, *ApJ*, 555, 489.
- Özel, F., Psaltis, D., Narayan, R., & Santos Villarreal, A. 2012, *ApJ*, 757, 55
- Özel, F., Psaltis, D., Narayan, R., & McClintock, J. E. 2010, *ApJ*, 725, 1918
- Paczynski, B. 1976, *Structure and Evolution of Close Binary Systems*, 75.
- Poleski, R. 2013, arXiv e-prints, arXiv:1306.2945
- Remillard, R. A., & McClintock, J. E. 2006, *ARA&A*, 44, 49
- Sana, H., de Mink, S. E., de Koter, A., et al. 2012, *Science*, 337, 444.
- Scalo, J. M. 1986, *FCPh*, 11, 1.
- Song, Y.-H., Luo, A.-L., Comte, G., et al. 2012, *Research in Astronomy and Astrophysics*, 12, 453
- Spitzer, L. 1978, *A Wiley-Interscience Publication*
- Su, D.-Q., & Cui, X.-Q. 2004, *ChJA&A*, 4, 1
- Thompson, T. A., Kochanek, C. S., Stanek, K. Z., et al. 2018, arXiv e-prints, arXiv:1806.02751
- Timmes, F. X., Woosley, S. E., & Weaver, T. A. 1996, *ApJ*, 457, 834
- van den Heuvel, E. P. J. 1992, *Environment Observation and Climate Modelling Through International Space Projects*,

- Wyrzykowski, L., Kostrzewa-Rutkowska, Z., Skowron, J., et al. 2016, *MNRAS*, 458, 3012
- Wu, Y., Luo, A.-L., Li, H.-N., et al. 2011, *Research in Astronomy and Astrophysics*, 11, 924
- Wu, Y., Du, B., Luo, A., et al. 2014, *Statistical Challenges in 21st Century Cosmology*, 340
- Wu, J., Orosz, J. A., McClintock, J. E., et al. 2016, *ApJ*, 825, 46.
- Xiang, M. S., Liu, X. W., Yuan, H. B., et al. 2015, *MNRAS*, 448, 822
- Yalinewich, A., Beniamini, P., Hotokezaka, K., & Zhu, W. 2018, *MNRAS*, 481, 930
- Yamaguchi, M. S., Kawanaka, N., Bulik, T., & Piran, T. 2018, *ApJ*, 861, 21
- Yuan, H., Liu, X., Xiang, M., et al. 2015, *ApJ*, 799, 135
- Yungelson, L. R., Lasota, J.-P., Nelemans, G., et al. 2006, *A&A*, 454, 559.
- Zhao, G., Zhao, Y.-H., Chu, Y.-Q., et al. 2012, *Research in Astronomy and Astrophysics*, 12, 723
- Zheng, L.-L., Gu, W.-M., Yi, T., et al. 2019, *AJ*, in press, arXiv:1909.06392
- Zong, W., Fu, J.-N., De Cat, P., et al. 2018, *ApJS*, 238, 30